Deep–Sea Research II xxx (xxxx) xxx

Contents lists available at ScienceDirect

Deep-Sea Research Part II

journal homepage: www.elsevier.com/locate/dsr2

Of Atlantic Meridional Overturning Circulation in the CMIP6 Project

Xun Gong [a,b,c], Hailong Liu [d,*], Fuchang Wang [e,f], Céline Heuzé [g]

[a] Institute for Advanced Marine Research, China University of Geosciences, Guangzhou, China
[b] State Key Laboratory of Biogeology and Environmental Geology, Hubei Key Laboratory of Marine Geological Resources, China University of Geosciences, Wuhan, China
[c] Shandong Provincial Key Laboratory of Computer Networks, Qilu University of Technology (Shandong Academy of Sciences), Jinan, China
[d] School of Oceanography, Shanghai Jiao Tong University, Shanghai, China
[e] Shanghai Typhoon Institute (STI) of China Meteorological Administration (CMA), Shanghai, China
[f] Department of Atmospheric and Oceanic Sciences and Institute of Atmospheric Sciences, Fudan University, Shanghai, China
[g] Department of Earth Sciences, University of Gothenburg, Gothenburg, Sweden

ARTICLE INFO

Keywords:
AMOC
CMIP6
Historical experiment
Trend and variability

ABSTRACT

The Atlantic Meridional Overturning Circulation (AMOC) upper-cell circulation is widely linked to global oceans and climate. Here, we focus on a statistical overview about the modelled AMOCs on the basis of the historical simulations in the 5th and 6th phase of the Coupled Model Intercomparison Project (CMIP5 and CMIP6), including the modelled AMOC strength, cell structure, long-term trend and the variabilities on interannual, decadal and multi-decadal scales. Our results show that the multi-model averaged AMOC mean state of CMIP5 is insignificantly different from the CMIP6 results, meanwhile the corresponding multi-model averaged AMOC variability is reduced from CMIP5 to CMIP6 results. Moreover, the CMIP6 multi-model averaged AMOC becomes further distinct from the mean state of Rapid Climate Change (RAPID) observations. Overall, 7 out of the 18 CMIP6 models have suggested AMOC strengthening, meanwhile 6 models have indicated declining trends in the AMOC, with the rest 5 models in the variabilities with insignificant trends. Overall, the CMIP6 results have suggested pronounced modelling discrepancies in revealing AMOC trends, distinct from the more commonly weakening trend of the AMOCs in the CMIP5 simulations. Moreover, the multi-model averaged AMOC variabilities are comparable between CMIP5 and CMIP6 simulations, on inter-annual, decadal and multi-decadal time scales, with the discrepancies remaining among models.

1Introduction

Atlantic Meridional Overturning Circulation (AMOC) refers to a zonal integration of water mass transport by the Atlantic ocean circulation. Meridionally, the upper-cell AMOC delivers low-latitude water of relatively higher temperatures and salinities to the subarctic ocean (Talley et al., 2003; Cunningham et al., 2007), and plays key roles in driving oceanic and climatic change not only within the Atlantic sector but also globally, via the coupled ocean-atmosphere -cryosphere system (e.g. Vellinga and Wood (2008); Drijfhout (2015)]. The downward branch of the AMOC upper cell, associated with the formation of North Atlantic deep-water (NADW) in the subpolar North Atlantic Ocean and Nordic Seas, acts as a main channel for the surface and deep-ocean heat exchange, effectively modulating ocean heat content and thus the ongoing global warming (e.g. Caesar et al., 2018; Chen and Tung, 2018; Tung and Chen, 2018). In parallel, AMOC impacts on global warming via modulating atmospheric CO_2 concentrations, by controlling air-sea CO_2 flux through physical and also biogeochemical processes coupled with the global carbon cycle (e.g. Honjo et al., 2014; Nielsen et al., 2019). Overall, AMOC processes are critical in shaping the background climate and the global warming.

Studies have investigated the AMOC processes and the associated physics using both modelling and observation approaches. In the 5th phase of the Coupled Model Intercomparison Project (CMIP5), numerical simulations using 23 models have suggested generally weakening trends of the AMOCs by different magnitudes, together with non-uniformed AMOC oscillations on decadal and multi-decadal time scales, based on the same set-up of historical increase in atmospheric greenhouse-gas concentrations since year 1850 (e.g. Cheng et al., 2013; Cheng et al., 2016; Heuzé, 2017; Yan et al., 2018; Hu et al., 2020; Weijer et al., 2020). Here, among the CMIP5 simulations, the distinct performance in AMOC oscillations acts as a statistic reason for the different

* Corresponding author.
E-mail address: hailong.liu@sjtu.edu.cn (H. Liu).

https://doi.org/10.1016/j.dsr2.2022.105193
Received 8 December 2021; Received in revised form 7 September 2022; Accepted 16 September 2022
Available online 29 September 2022

AMOC long-term trends (e.g. Knutti and Sedláček, 2013). In particular, Xu et al. (2019) have suggested that the disagreement in simulating AMOC multi-decadal variability among simulations is a cause of the non-uniform AMOC trends since year 1850 based on historical set-ups. In parallel, the in-situ data by the physical oceanography observations on the AMOC is only available for the past less than 20 years (Kanzow et al., 2010; Johns et al., 2011; Smeed, 2018; Frajka-Williams, 2019). In addition, modelling simulations have shown AMOC variability with amplitudes generally less than the analysis based on the observation data of ocean temperatures, sea level pressures and Rapid Climate Change (RAPID) monitoring results, in particular on multi-decadal timescales (Roberts et al., 2014; Kim et al., 2018; Yan et al., 2018). Therefore, the AMOC variability across time scales with long-term trend due to the ongoing global warming remains unclear, and we will further develop the understanding based on the analysis of CMIP6 simulations.

In this study, we aim to provide essential information and statistics about the AMOC structure, trend and variabilities in the CMIP6 simulations, with the focus on the modelled AMOC change from CMIP5 to CMIP6. It is necessary to understand the diversities about global background oceans and climate states, and then processes within the ocean-atmosphere-cryosphere coupled system, among the CMIP6 simulations. Specifically, our analysis is based on 18 paired simulations using the same models but different versions in the CMIP5 and CMIP6. Notably, from CMIP5 to CMIP6, each model has been developed via changing distinct aspect individually. Moreover, rather than to discuss the physics for the AMOC change in each pair of modelling simulations, we make comparison and provide an overview about the computed AMOCs from the CMIP5 to CMIP6 projects. This effort will benefit the studies about modelling intercomparison between CMIP5 and CMIP6, or among CMIP6 simulations, e.g. in this special issue.

2Data and methodology

2.1Observational and model datasets

In CMIP6, total 48 historical-scenario simulations (https://pcmdi.llnl.gov/CMIP6) are conducted using 23 ESMs (Table 1). In this work, simulations using 18 Earth System Models commonly existing in the CMIP5 and CMIP6 projects are analyzed with the focus on AMOC and the corresponding North Atlantic climates, based on the modelling output of AMOC stream function, mixed layer depths (MLD), sea level pressures (SLP) and sea surface temperatures (SST). The CMIP6 historical runs are forced by the common atmospheric greenhouse gas compositions from year 1850–2014 (O'Neill et al., 2014), starting from individual quasi-equilibrium of preindustrial-control state, as designed in the CMIP6 protocol (Eyring et al., 2016). In comparison, the CMIP5 historical runs are forced by a transition using the same atmospheric greenhouse gas compositions but from year 1850–2005 (Van Vuuren and Riahi, 2011; Taylor et al., 2012).

In our analysis, the data, including MLD, SLP and SST, have been interpolated to a $1^\circ \times 1^\circ$ grid from model-individually different horizontal resolutions using bilinear interpolation approach, while keeping their monthly time resolution. Moreover, the calculation of the North Atlantic Oscillation (NAO) index is based on the algorithm https://www.ncdc.noaa.gov/teleconnections/nao. Furthermore, an approach of *t*-test with 90% significance level is applied for intercomparisons of AMOC timeseries among CMIP5, CMIP6 simulations and Observations.

In addition, the AMOC strength timeseries is calculated based on the maximum stream function values at 26°N (AMOC-26Nmax, thereafter (Duchez et al., 2014), and a basin-wide averaged AMOC index refers to the mean of AMOC strength between 30S and 60N (AMOC-ALTmean, thereafter, c.f. Xu et al., 2019). Here, the AMOC-ALTmean index is calculated as the meridional average of the stream function maximum in the AMOC upper cell at each latitude between 30S and 60N. In our analysis, variability refers to the temporal standard deviations in different indexes.

To assess the AMOC variability across time scales, we decompose the AMOC strength timeseries to 7 intrinsic mode functions (IMFs) by applying the Ensemble Empirical Mode Decomposition (EEMD) algorithm (Huang and Wu 2008; Wu and Huang 2009), with the focus on interannual, decadal and multi-decadal time scales and a long-term trend through the historical interval. In details, IMF1 to IMF6 are about the total and its variabilities on 3, 7, 16 and 42, 61 and 182 years, while IMF7 is for the remaining long-term signal. In addition, the AMOC variabilities on interannual, decadal and multi-decadal scales are calculated by [IMF2 + IMF3], IMF4 and [IMF5 + IMF6], respectively.

3Results and Discussions

Within the 18 ESMs in the CMIP5 and CMIP6 projects, the AMOC-26Nmax time series show large diversities in its long-term trend, and variabilities, as well as AMOC cell's geographic structures (Fig. 1 and Tab.2).

3.1AMOC cell

In the CMIP6 project, 11 models show stronger AMOC in the mean state and 13 models exhibit larger AMOC variability, compared to the CMIP5 results, based on the AMOC-26Nmax index (Table 2). In year 1850–2005, the multi-model averaged AMOC mean state is 18.6 ± 4.2 Sv, and the multi-model averaged variability is 1.4 ± 0.5 Sv. In comparison, the values in the CMIP5 simulations are 17.5 ± 4.7 Sv and 1.0 ± 0.3 Sv, respectively. On the basis of *t*-test approach, the multi-model averaged AMOC mean state of CMIP5 is insignificantly different from the CMIP6 results, meanwhile the corresponding multi-model averaged AMOC variability is reduced from CMIP5 to CMIP6 results.

Therefore, the CMIP6 simulations have suggested relatively stronger AMOC in the mean state and comparable variability magnitude, relative to the CMIP5 results. It is virtually the same, when the CMIP6 calculation of AMOC-26Nmax is based on year 1850–2014 (18.4 ± 4.4 Sv for the mean state, and 1.0 ± 0.5 Sv for the variability). Moreover, on the basis of AMOC-26Nmax index, only for MIROC5 model in CMIP5 project and HadGEM3-GC31-LL in CMIP6 project the calculated AMOC mean states insignificantly differ from the RAPID mean-state value during year 2004–2017, meanwhile the rest models showed significant difference (Tab S2). However, regarding the multi-model averaged AMOC mean state, the differences among CMIP6, CMIP5 and RAPID remain within their temporal standard deviations.

About the AMOC upper cell's depth range, the multi-model averaged AMOC depth in the CMIP6 is 3405 ± 786 m, relatively deeper than 3143 ± 494 m in the CMIP5 result (Tab. S1 and Fig. S3), and much shallower than ~5000 m in the RAPID observation (McCarthy, 2015). Here, the bottom of AMOC upper cell is referred to the zero-value line in the AMOC stream function at 26°N. In general, although the depth of AMOC upper cell varies along latitudes, the AMOC becomes deeper when it gets stronger in most CMIP5 and CMIP6 simulations (Fig. 1). On the other hand, some models (e.g. MRI-ESM, IPSL and CNRM) show stronger AMOC but comparable cell depths from the CMIP5 to CMIP6. Qualitatively, CMIP5 and CMIP6 modelling simulations have suggested a linkage between AMOC strength and cell depths (Tab. S1). Besides the CMIP5 and CMIP6 project, modelling results in Paleoclimate Modelling Intercomparison Projects II, III and IV (PMIP2, 3 and 4 projects) have shown the similar concurrence between AMOC acceleration and its deepening, although based on a different background climate from the modern conditions, e.g. the Last Glacial Maximum (Otto-Bliesner et al., 2007; Kageyama et al., 2021). Alternatively, a study has suggested that the change in the Antarctic Bottom Water formation and extension, i.e. the lower branch of Atlantic circulation cell, may cause the decoupling of AMOC strengthening from its cell deepening, by squeezing the AMOC upper cell, based on the LGM oceans (c.f. Zhang et al., 2013).

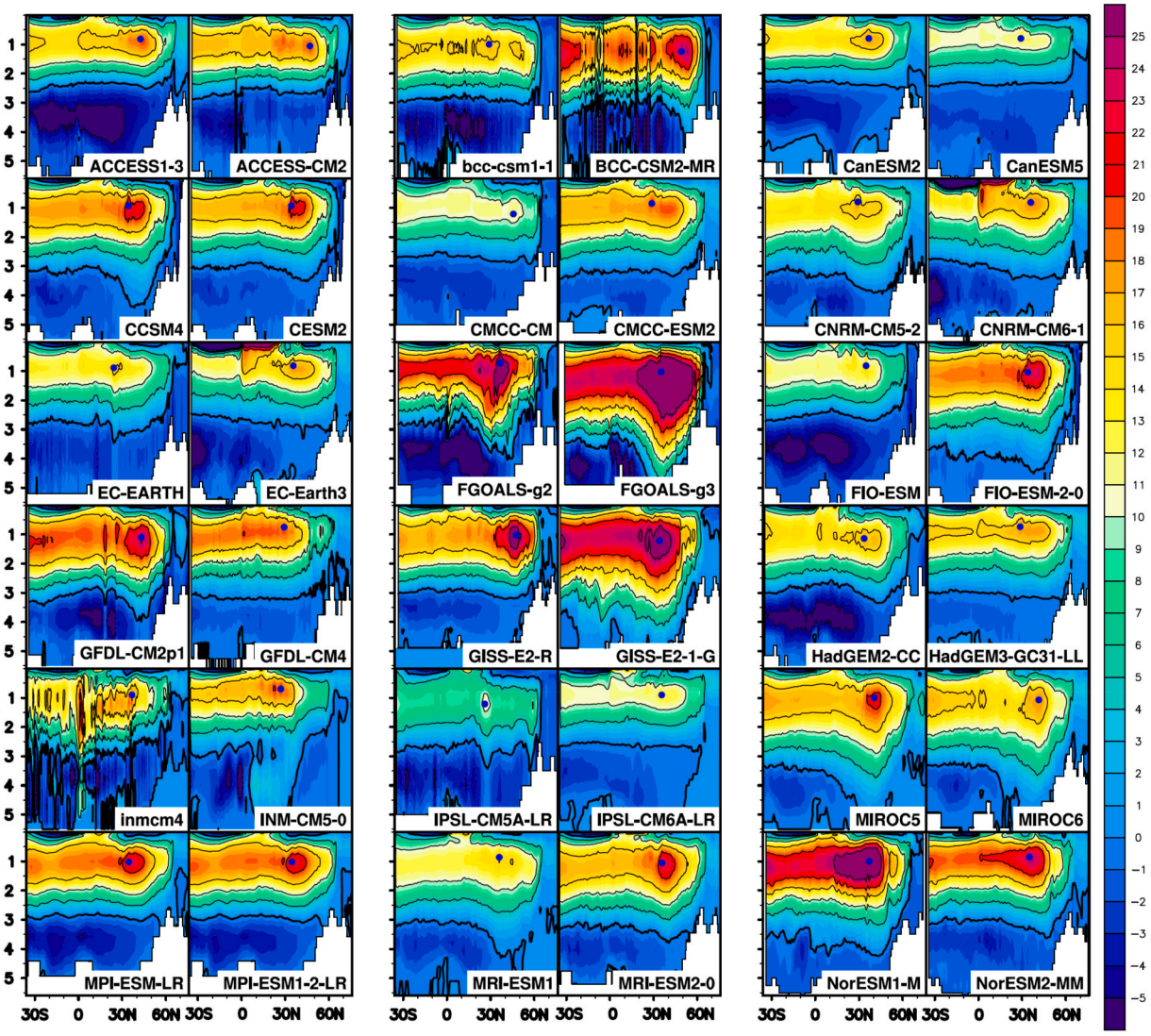

Fig. 1. Modelled AMOC in CMIP5 and CMIP6 simulations. In each column, the left and right panels show the results using CMIP5 and CMIP6 model versions, respectively. Color shadings explain the stream function in the unit of Sverdrup (Sv, 1 Sv = 10^6 m^3/s), and thick black lines show zero values of the stream function. In addition, blue dots indicate the position of the maximum value in the AMOC upper cell.

3.2AMOC trends

In the CMIP5 results, most simulations have suggested a declining AMOC based on historical set-ups, meanwhile there is no common AMOC trend in the CMIP6 simulations (Figs. 2 and 6). Based on proxy-based reconstructions, Thornalley et al., (2018) have suggested a gradual, continued AMOC weakening over the past 150 years. In contrast, Parker and Ollier (2016) have concluded no clear trend outside the inter-annual and multi-decadal variability in the direction of increasing or decreasing strength over the last decades, using tide gauge data complementing recent satellite and ocean sensor observations, mainly due to the observation uncertainties and time coverage. Furthermore, solely from observations, Fraser and Cunningham (2021) have characterized multidecadal oscillation as the dominant pattern in AMOC variation over the last 120 years. It is similar to the result of no evidence for a long-term trend in AMOC over the last 70–100 years using the extensive hydrographic records by Rossby et al., (2020). However, Caesar et al., (2018) have indicated a likely ~3 Sv linear weakening over the 136 years on the basis of high-resolution climate model results, while Rahmstorf et al., (2015) have suggested an AMOC reduction over the twentieth century, using the results of different climate models. Also using modelling approach, Menary et al., (2013) and Weijer et al. (2020) have indicated that the competing effect by greenhouse gases and aerosol forcings is a likely cause in disturbing the simulation of AMOC variations. Overall, paleoceanographic studies have not reached a conclusion about whether there is a long-term AMOC trend since year 1850 or in the last century, in line with the CMIP6 multi-model results.

In addition, the CMIP6 simulations have shown pronounced inter-model discrepancies in the long-term AMOC trend. On one hand, the increase in atmospheric CO_2 concentrations would act to reduce the NADW formation and thus a weakening of AMOC, via enhancing upper-ocean stratification and retreating sea ice, by increasing SST (e.g. Capotondi et al., 2012). This physical process, however, relies on whether the surface-warming due to historical increase of the atmospheric CO_2 concentrations is strong enough to change the ocean stratification in the initial conditions of each simulation significantly. In CMIP5 and CMIP6 projects, each simulation is initialized by its own preindustrial-control quasi-equilibrium state that is different from each other. These distinct initial conditions contribute to the model-dependent responses in AMOC trend (in spite of the same forcing of historical set-up), besides the parameterization (e.g. Oka et al., 2012; Gong et al., 2013; Gong et al., 2015). In a historical simulation, when vertical temperature structure is not the determining factor in density stratification, the global warming will only perturb AMOC variabilities,

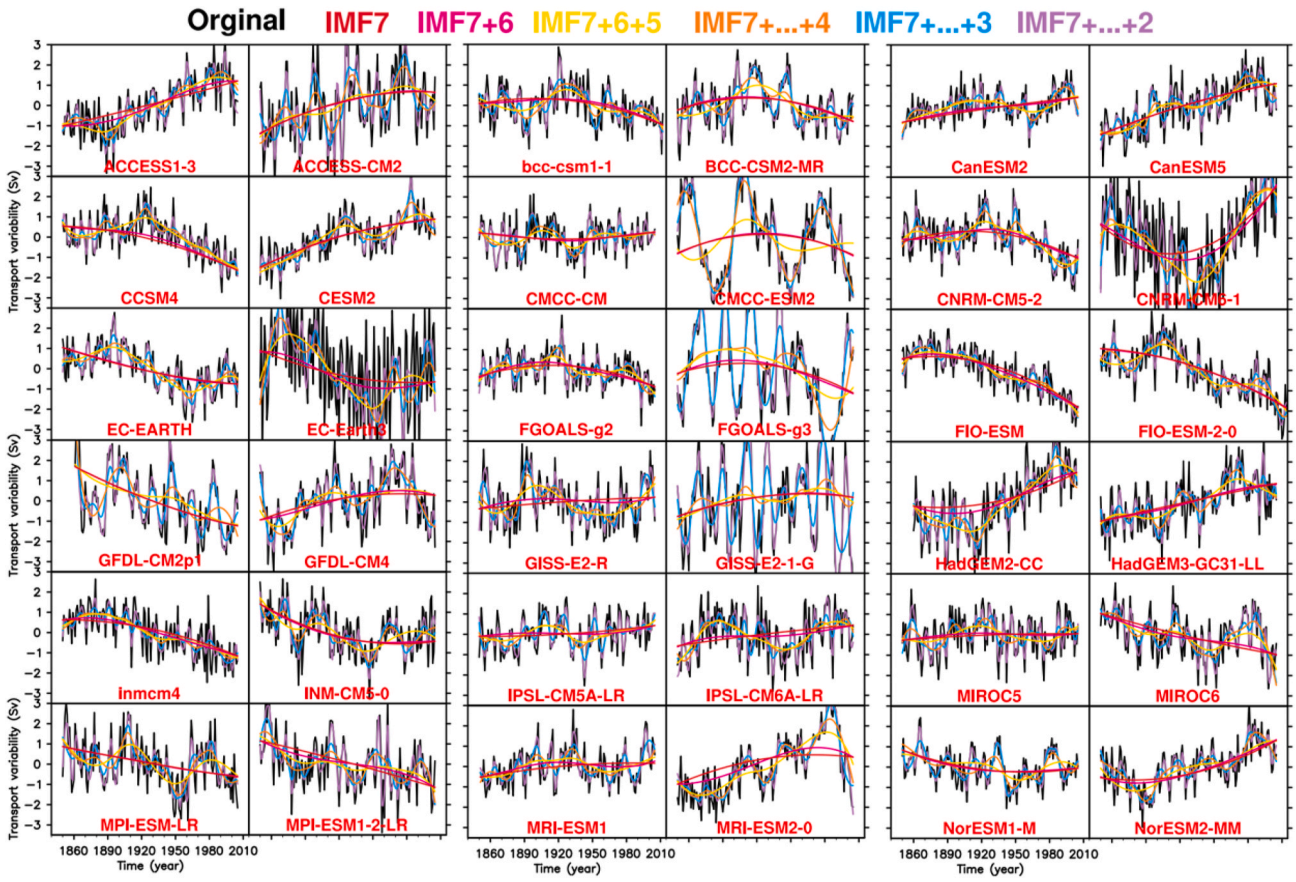

Fig. 2. EEMD-decomposited AMOC (AMOC-26Nmax index) variabilities in CMIP5 and CMIP6 simulations. As in Fig. 1, Left and right panels in each column show the results using CMIP5 and CMIP6 model versions, respectively.

rather than causing a long-term trend. In this situation, a longer integration time will be required to shift AMOC significantly. Furthermore, most CMIP5 simulations have characterized similar SST trends averaged over 50°S - 65°N in the global ocean (Jha et al., 2014), coherent with the commonly AMOC declining trends. In comparison, the same SST calculation based on the CMIP6 simulations has suggested similar warming trends but with relatively larger discrepancies, potentially explaining (at least in part) the large spread of the corresponding AMOC trends spanning from weakening to strengthening (Fig. S1). In particular, the CMIP5-to-CMIP6 enlarged discrepancies in the SST averaged over the latitude range of 50°S - 65°N in the Atlantic Ocean becomes pronounced, compared to the calculation in the global ocean. It also indicates potential importance of deeper-ocean conditions in reproducing the AMOC during the historical interval.

3.3AMOC variability

The CMIP5 and CMIP6 simulations have commonly suggested the existence of AMOC variabilities on interannual and decadal and multi-decadal time scales (Fig. 3). From CMIP5 to CMIP6, 11 of the 18 models show stronger AMOC variability on the multi-decadal time scales, meanwhile the rest 7 models exhibit either comparable or reduced magnitudes in the variability. In parallel, the AMOC variability on the inter-annual scale becomes larger in 9 CMIP6 models; on decadal time scales, different 9 models out of the total 18 have suggested larger magnitudes in CMIP6 than CMIP5. Statistically, the multi-model averaged AMOC variabilities are comparable in the CMIP5 and CMIP6 results on inter-annual, decadal and multi-decadal time scales, but with large discrepancies among CMIP6 models.

Previous studies have attributed the diversity in AMOC multi-decadal variabilities to distinct behavior of NAO processes (Wang et al., 2017; Peings et al., 2016). For instance, Xu et al. (2019) have suggested that a stronger NAO variability plays a role in enlarging the corresponding AMOC variability amplitude. Here, we provide a compilation about the NAO index and NAO-AMOC relationship in CMIP5 and CMIP6 simulations. From the CMIP5 to CMIP6, each model development has shown various changes in the NAO-AMOC relationship on multi-decadal time scales (Fig. 4). In the CMIP6, 5 simulations calculate a strong NAO-AMOC correlation with the correlation coefficient larger than 0.5 (Table 2). Similarly, also 5 but different models have suggested strong NAO-AMOC correlation in the CMIP5 results. On average, the CMIP5 and CMIP6 models have similarly suggested the NAO-AMOC correlation coefficient value of ~0.4, with NAO leading AMOC change by 8–12 years. Notably, the CESM2 simulation shows the strongest link between NAO and AMOC (correlation coefficient equals to 0.8) among all the CMIP5 and CMIP6 models. Similar with the result on the multi-decadal time scales, the multi-model averaged NAO-AMOC correlation on decadal and inter-annual scales in the CMIP6 simulations are comparable with the CMIP5 results, but the change due to CMIP5-to-CMIP6 model development is divided among models (Fig. s4-s6). According to our analysis, a stronger NAO-AMOC correlation does not necessarily have to accompany with larger variability amplitudes of the AMOC and NAO. This finding is in line with the findings of Xu et al. (2019) based on the CMIP5 results, likely attributed to the lack of substantial improvement in simulating NAO from CMIP5 to CMIP6 due to the known biases such as an overly zonal flows by climate models (c.f. Davini and D'Andrea, 2016).

Moreover, the CMIP6 simulations have characterized AMOC variability on the multi-decadal time scale by largest amplitudes at 20–60°N, where the North Atlantic deep-water formation occurs and overlapping

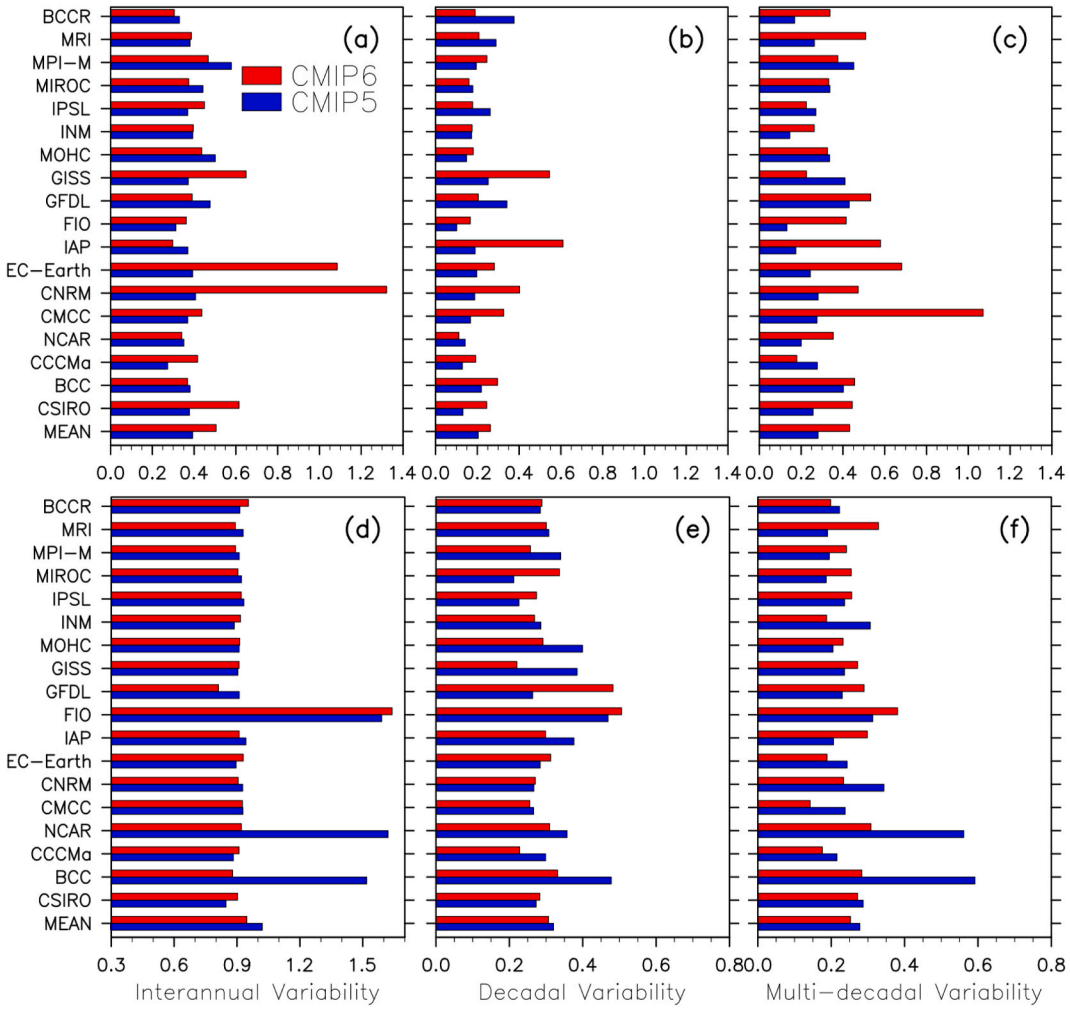

Fig. 3. Modelled NAO and AMOC (AMOC-26Nmax index) variabilities on interannual, decadal and multi-decadal time scales in CMIP5 and CMIP6 simulations. Upper and Lower rows show the AMOC and NAO variabilities, respectively. Left, middle and right columns exhibit the interannual, decadal and multi-decadal scale variabilities, respectively. In each panel, MEAN is for the multi-model average.

with the northern hemisphere westerlies (Fig. 5). Relative to the CMIP5 results, the CMIP6 multi-model averaged AMOC variability at 20–60°N is further enlarged. Similar to the multi-decadal time scale, AMOC variability on the decadal time scale also shows the largest amplitudes at 20–60°N in the CMIP6 simulations, developing from the CMIP5 results. On the other hand, CMIP5-to-CMIP6 change of the AMOC variability across latitudes is different from model to model on decadal time scale, as well as on multi-decadal scale (Fig. 5b). It might be a reason for the disagreement about long-term AMOC trend in the CMIP5 to CMIP6 simulations.

In addition, our analysis about interannual-scale AMOC variability has characterized that the multi-model averaged AMOC variability shows larger amplitudes throughout 20°S to 60°N in the CMIP6 results, compared to the CMIP5 (Fig. 5). This is similar for the variation in the AMOC variability on the decadal and multi-decadal time scales. It is likely due to the pacing process of the El Niño-Southern Oscillation (ENSO) processes in the Atlantic sector, also known as the Atlantic Zonal Mode or Atlantic Niño processes and its propagation within the atmosphere-ocean coupled system (e.g. Zebiak, 1993; Latif and Grötzner, 2000; Keenlyside and Latif, 2007). Yet, changes in Atlantic Niño from CMIP5 to CMIP6 remains to be studied.

Besides, we have calculated the correlation between the AMOC strength averaged over the latitude bands with the AMOC-ALTmean index, aiming for a diagnose about meridional coherence in AMOC variability. In the CMIP6 simulations, the correlation values are always larger than 0.65 between 0°S and 40°N and then rapidly decreases towards both poles commonly on interannual and decadal time scales. It is different from the existence of peak values at low latitudes (20°S to 20°N) on the multi-decadal time scales (Fig. 5), with inter-model inconsistence (Fig. s2). Similarly, the across-time scale inconsistence in the meridional patterns of the correlations between the latitude-band averaged AMOC and the AMOC-ALTmean index are also characterized in the CMIP6 simulations. It suggests distinct roles of the climate processes along latitudes in changing the basin-scale AMOC oscillations.

4Summary and discussion

In this study, we focus on statistical intercomparison about the modelled AMOC strength, cell structure, long-term trend during the historical interval and the variabilities across interannual, decadal and multi-decadal time scales in the CMIP5 and CMIP6 projects, as well as a comparison to the observations and paleoceanographic evidences. Totally, simulations using 18 models that commonly exist in the CMIP5 and CMIP6 projects but of different versions are involved in our analysis.

In our results, the multi-model averaged AMOC in the CMIP6 project become relatively stronger and deeper than the CMIP5 results, and relatively further distinct from the physical oceanography observations, within the uncertainty due to their temporal standard deviations. Moreover, there is no common AMOC trend on the basis of the CMIP6 simulations, different from a declining AMOC suggested by most

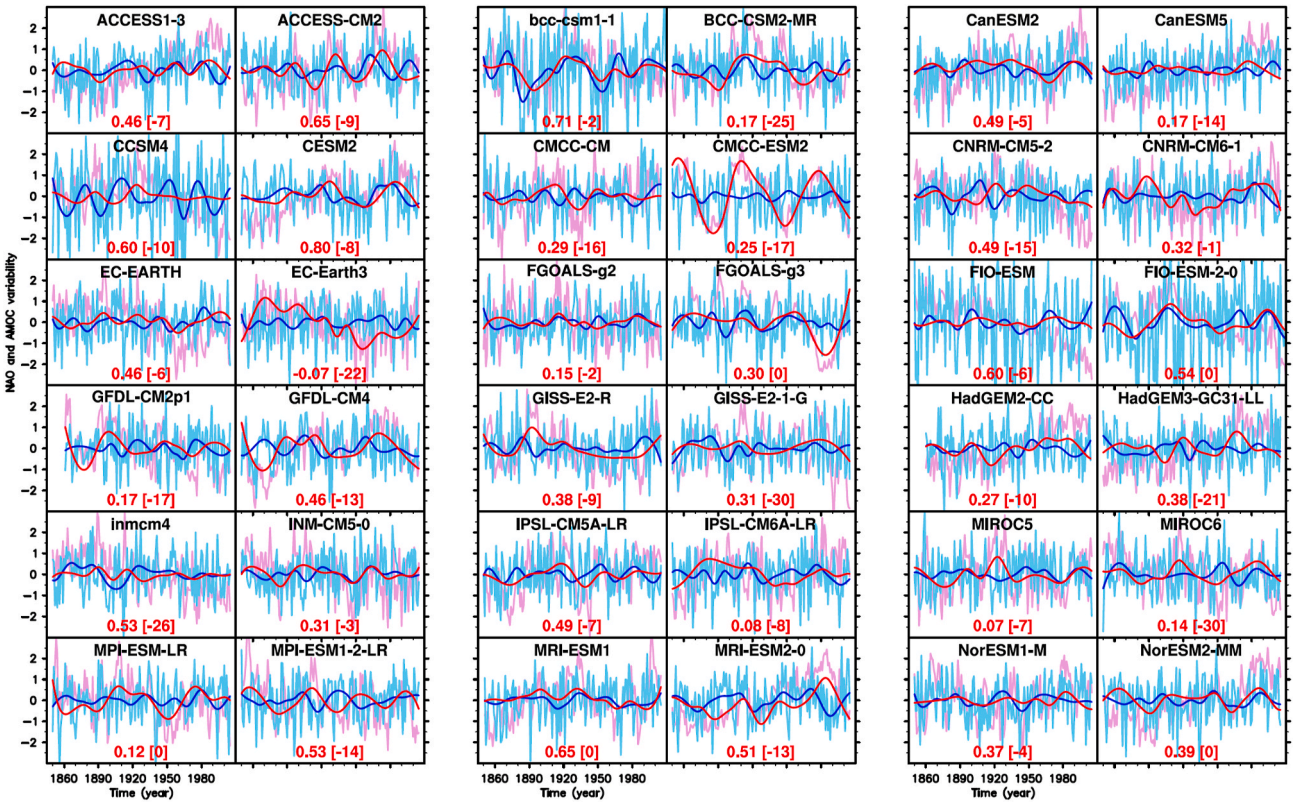

Fig. 4. Modelled AMOC (AMOC-26Nmax index), NAO indexes and the NAO-AMOC correlation on multi-decadal time scale, in CMIP5 and CMIP6 simulations. The original AMOC (light red) and NAO (light blue) indexes are plotted and overlapped by EEMD-decomposited, multi-decadal scale variabilities in AMOC (dark red) and NAO (dark blue). In each panel, numbers show the maximum correlation coefficient and the associated lead/lag years (in bracket), with negative values denoting that NAO leads AMOC change.

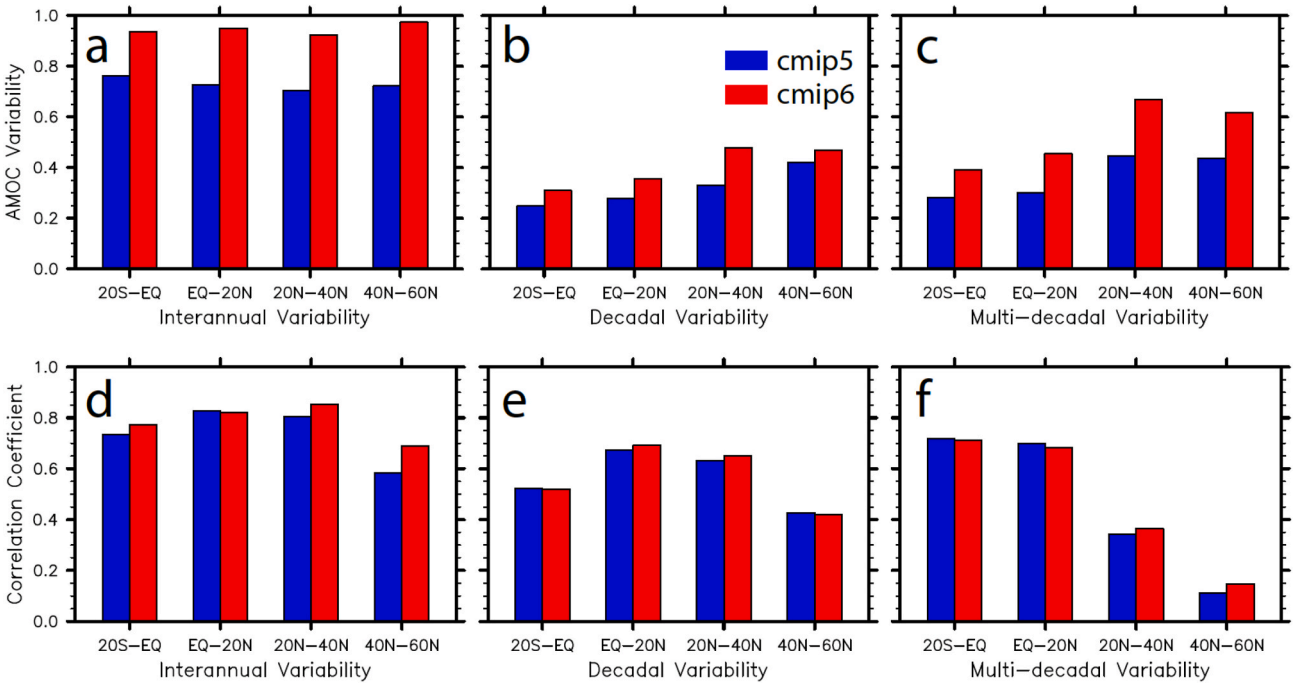

Fig. 5. Multi-model average of the AMOC variability in the latitude bands and their correlations with AMOC-ALTmean index, on interannual, decadal and multi-decadal time scales, in the CMIP5 and CMIP6 simulations. Here, AMOC variability refers to the temporal standard deviation of the AMOC index, which is firstly calculated at each latitude using the algorithm resembling the AMOC-26Nmax index, and then averaged in the corresponding latitude band. Upper and Lower rows are for the multi-model averaged AMOC Variability along with latitudes and their correlations with the basin-wide AMOC indexes, respectively. Left, middle and right columns exhibit the variabilities on interannual, decadal and multi-decadal time scales, respectively.

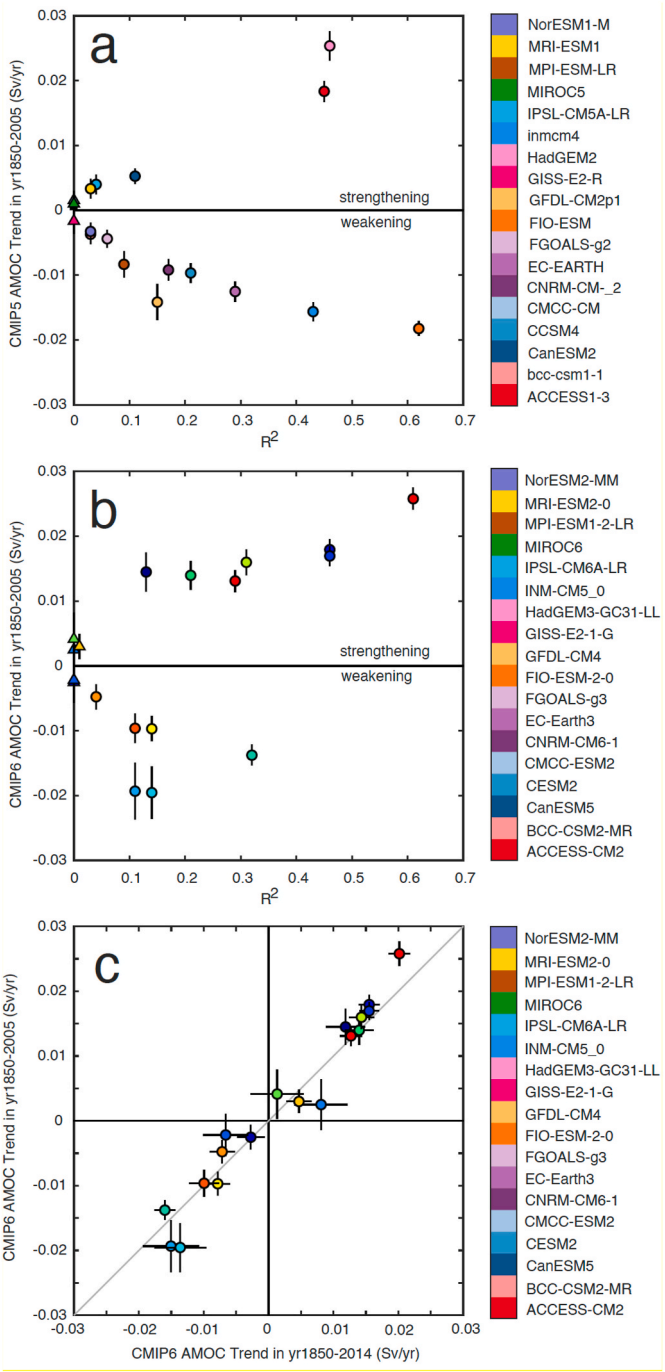

Fig. 6. Modelled AMOC trends in CMIP5 and CMIP6 projects, based on the AMOC-26Nmax index by applying linear regression approach. The R^2 and p-value are the statistics for the fitting trend in the linear regression calculation. a, b show the AMOC trends of year 1850–2005 in the CMIP5 and CMIP6 projects, respectively. c exhibits the AMOC trends in the different periods of year 1850–2005 and year 1850–2014, in the CMIP6 project. In a and b, the triangle and round signs illustrate the p-values larger and smaller than 0.05, respectively. A CMIP5 model and its corresponding CMIP6 version is indicated by the same color.

simulations in the CMIP5 results. Therefore, regarding the calculation of the historical AMOC mean state, the CMIP6 result is not improved from the CMIP5. Furthermore, the AMOC variabilities on interannual, decadal and multi-decadal time scales show insignificant changes between the CMIP5 to CMIP6 project, and the inter-model spread becomes larger from CMIP5 to CMIP6.

Our results show that a stronger NAO-AMOC correlation is not necessarily accompanied with larger variability amplitudes in NAO and AMOC variability on the multi-decadal time scales, suggesting that the NAO is not the only factor in regulating AMOC multi-decadal variability (e.g. Stouffer et al., 2006; Haskins et al., 2019; Xu et al., 2019). This is alternative to the hypothesis that AMOC is the response of upper ocean to NAO through subpolar gyre and Labrador Sea (Delworth and Zeng, 2016; Wang et al., 2017). In addition, Sidorenko et al. (2021) has indicated that the NAO-AMOC linkage is more obvious in isopycnal than in depth framework for their model, providing a new perspective to be testified in CMIP models. Notably, the modelling circumstance that a stronger NAO-AMOC correlation does not have to accompany larger AMOC and NAO variability amplitudes is based on the fact that the NAO-controlled AMOC variability on the multi-decadal time scales likely remains underestimated in the CMIP6 models (c.f. Wen et al., 2016; Seip et al., 2019). It has been argued that the NAO-AMOC relationship is not stable but varies with years, even sometimes takes place through the Atlantic multidecadal oscillation (Seip et al., 2019). Here, we suggest to involve both NAO and Atlantic multidecadal oscillation in analyzing the AMOC variability on the multi-decadal scales, as a future perspective.

From CMIP5 to CMIP6, the models are developed by better model configurations and more reasonable physics description, e.g. overflow parameterization in CESM models (Danabasoglu et al., 2010; Yeager and Danabasoglu, 2012) and implement of parameterization for shallow convective processes and stratosphere in MIROC models (Tatebe et al., 2019), while they also use similar resolutions (GFDL in CMIP6 applies a much higher resolution than the rest models, Tab.1). A higher model resolution tends to induce stronger AMOC (Hirschi et al., 2020; Roberts et al., 2020), likely caused by more intense air-sea interaction. In addition, the sensitivity of AMOC variability to model resolution in CMIP models need further investigation.

In addition, our analysis focuses on a statistical overview about the AMOC change due to the modelling development from CMIP5 to CMIP6, rather than the exploration of determination physics for the AMOC change in each model and their complexity among models. On the other hand, in our results, inter-model discrepancies of AMOC strength exist in concurrence with various AMOC cell structures, indicating a linkage between spatial and temporal evolution in AMOCs. At this point, wesuggest a future perspective for model development and thus experiments on the basis of vertical (at least in deep oceans) density stratifications that resemble the modern reconstructions, using CMIP models. This is a likely way to constrain inter-model discrepancies in AMOC calculation, worth to be tested.

Here, our compilation of the modelled AMOC states and change are important to understand CMIP5-to-CMIP6 anomalies in almost all the climatic processes, and useful to the discussion about the CMIP6 results by other papers in this special issue. Reversely, we believe that the other studies of this special issue also offer clues to understand the mechanism for the AMOC inconsistence from the CMIP5 to CMIP6 project.

Author statement

Xun Gong: Methodology, Analysis, Writing-Revising , Original draft preparation. **Hailong Liu**: Conceptualization, Analysis, Writing-Revising andEditing **Fuchang Wang**: Data Preparation, Calculation, Analysis, Writing- Revising and Editing. **Celine Heuze**, Analysis, Writing- Revising and Editing.

Declaration of competing interest

The authors declare the following financial interests/personal relationships which may be considered as potential competing interests: Hailong Liu reports financial support was provided by National Natural Science Foundation of China. Xun Gong reports financial support was provided by the MOST funding National Key R&D Program of China

(2019YFE0125000)

Data availability

i have shared the link to my data/code at the Attach File step.

Acknowledgments

Our application of t-test and EEMD approaches are based on MATLAB v.R2021b and NCL language v. 6.6.2, respectively. We thank Prof. Xiaobiao Xu for the valuable suggestion. We thank the climate modelling groups for producing and making available their model output, the Earth System Grid Federation (ESGF) for archiving and providing access to data, and the multiple funding agencies which support CMIP and ESGF. All CMIP data are available from the ESGF at https://esgf-data.dkrz.de/search/cmip5-dkrz/and https://esgf-data.dkrz.de/search/cmip6-dkrz/. This work was supported by the MOST funding National Key R&D Program of China (2019YFE0125000), National Science Foundation of China 41861134040, 41776019, and Sino-German Mobility Program M0333. Data from the RAPID-WATCH MOC monitoring project are funded by theNatural Environment Research Council and are freely available from www.rapid.ac.uk/rapidmoc.

Appendix A. Supplementary data

Supplementary data to this article can be found online at https://doi.org/10.1016/j.dsr2.2022.105193.

Tab.1
The 18 pairs of models for CMIP r1i1p1 experiments that are used in this study.

	CMIP5	CMIP6	Model groups
	Layer * Lat * Lon		
1	ACCESS1-3 (50*300*360)	ACCESS-CM2 (50*300*360)	CSIRO (Commonwealth Scientific and Industrial Research Organisation), BOM (Bureau of Meteorology), ARCCSS (Australian Research Council Centre of Excellence for Climate System Science, Australia) Australia
2	bcc-csm1-1 (40*232*360)	BCC-CSM2-MR (40*232*360)	BCC (Beijing Climate Center, China)
3	CanESM2 (40*192*256)	CanESM5 (45*291*360)	CCCMa (Canadian Centre for Climate Modelling and Analysis, Canada)
4	CCSM4 (60*384*320)	CESM2 (60*384*320)	NCAR (National Center for Atmospheric Research, USA)
5	CMCC-CM (31*149*182)	CMCC-ESM2 (50*292*362)	CMCC (Fondazione Centro Euro-Mediterraneo sui Cambiamenti Climatici, Italy)
6	CNRM-CM5-2 (42*292*362)	CNRM-CM6-1 (75*294*362)	CNRM (Centre National de Recherches Meteorologiques, France); CERFACS (Centre Europeen de Recherche et de Formation Avancee en Calcul cientifique, France)
7	EC-EARTH (42*292*362)	EC-Earth3 (75*292*362)	EC-Earth-Consortium
8	FGOALS-g2 (30*196*360)	FGOALS-g3 (30*218*360)	IAP (Institute of Atmospheric Physics, China); THU(Tsinghua University, China)
9	FIO-ESM (40*384*320)	FIO-ESM-2-0 (60*384*320)	FIO (First Institute of Oceanography); QNLM (Qingdao National Laboratory for Marine Science and Technology), China
10	GFDL-CM2p1 (50*200*360)	GFDL-CM4 (35*1080*1440)	GFDL (Geophysical Fluid Dynamics Laboratory, USA)
11	GISS-E2-R (32*180*288)	GISS-E2-1-G (40*180*288)	GISS (Goddard Institute for Space Studies, USA)
12	HadGEM2-CC (40*216*360)	HadGEM3-GC31-LL (75*330*360)	MOHC (Met Office Hadley Centre, UK); INPE (Instituto Nacional de Pesquisas Espaciais, Brazil)
13	Inmcm4 (40*340*360)	INM-CM5-0 (33*180*360)	INM (Institute for Numerical Mathematics, Russian Academy of Science, Russia)
14	IPSL-CM5A-LR (31*149*182)	IPSL-CM6A-LR (75*332*362)	IPSL (Institut Pierre Simon Laplace, France)
15	MIROC5 (50*224*256)	MIROC6 (63*256*360)	University of Tokyo, JAMSTEC (Japan Agency for Marine-Earth Science and Technology), AORI (Atmosphere and Ocean Research Institute), NIES (National Institute for Environmental Studies), and R–CCS (RIKEN Center for Computational Science), Japan
16	MPI-ESM-LR (40*220*256)	MPI-ESM1-2-LR (40*220*256)	MPI-M (Max Planck Institute for Meteorology, Germany)
17	MRI-ESM1 (51*368*360)	MRI-ESM2-0 (61*363*360)	MRI (Meteorological Research Institute, Japan)
18	NorESM1-M (70*384*320)	NorESM2-MM (70*385*360)	BCCR (Bjerknes Centre for Climate Research); CICERO (Center for International Climate and Environmental Research); MET-Norway (Norwegian Meteorological Institute); NERSC (Nansen Environmental and Remote Sensing Center); NILU (Norwegian Institute for Air Research); UiB (University of Bergen); UiO (University of Oslo); UNI (Uni Research), Norway

Tab 2
Modelled NAO, AMOC strength (AMOC-26Nmax) and the NAO-AMOC correlation in the CMIP5 and CMIP6 simulations.

CMIP6, Year 1850–2005					CMIP5, Year 1850–2005				
Model	AMOC	NAO (EOF1, %)	Corr.	Lead/Lag,	Model	AMOC	NAO (EOF1, %)	Corr.	Lead/Lag,
	(Sv)		Coef.	AMOC		(Sv)		Coef.	AMOC
ACCESS-CM2	19.0 ± 1.6	45.0	0.65	−9	ACCESS1-3	16.0 ± 1.2	36.7	0.46	−7
	16.1 ± 1.1	35.9	0.17	−25	bcc-csm1-1	15.8 ± 0.9	40.0	0.71	−2

(continued on next page)

Tab 2 (*continued*)

CMIP6, Year 1850–2005					CMIP5, Year 1850–2005				
Model	AMOC	NAO (EOF1, %)	Corr.	Lead/ Lag,	Model	AMOC	NAO (EOF1, %)	Corr.	Lead/ Lag,
	(Sv)		Coef.	AMOC		(Sv)		Coef.	AMOC
BCC-CSM2-MR									
CanESM5	11.9 ± 1.1	44.6	0.17	−14	CanESM2	15.2 ± 0.7	33.7	0.49	−5
CESM2	18.0 ± 1.0	36.7	0.80	−8	CCSM4	18.7 ± 0.9	42.2	0.60	−10
CMCC-ESM2	18.4 ± 1.8	39.2	0.25	−17	CMCC-CM	11.6 ± 0.8	41.1	0.29	−16
CNRM-CM6-1	16.5 ± 2.1	47.7	0.32	−1	CNRM-CM5-2	16.2 ± 1.0	43.3	0.49	−15
EC-Earth3	15.3 ± 2.3	40.2	−0.07	−22	EC-Earth	15.7 ± 1.0	38.7	0.46	−6
FGOALS-g3	29.0 ± 2.2	43.5	0.30	0	FGOALS-g2	24.6 ± 0.8	34.4	0.15	−2
FIO-ESM-2-0	19.5 ± 1.2	45.6	0.54	0	FIO-ESM	14.6 ± 1.0	40.1	0.60	−6
GFDL-CM4	18.9 ± 1.3	38.6	0.46	−13	GFDL-CM2p1	21.9 ± 1.5	45.5	0.17	−17
GISS-E2-1-G	26.6 ± 2.1	37.9	0.31	−30	GISS-E2-R	18.7 ± 1.1	33.9	0.38	−9
HadGEM3-LL	17.0 ± 1.2	46.5	0.38	−21	HadGEM2-CC	14.8 ± 1.6	35.0	0.27	−10
INMM-CM5-0	19.9 ± 1.1	37.2	0.31	−3	Inmcm4	18.0 ± 1.1	36.7	0.53	−26
IPSL-CM6A-LR	12.9 ± 1.0	38.5	0.08	−8	IPSL-CM5A-LR	10.8 ± 0.8	44.2	0.49	−7
MIROC6	14.7 ± 1.1	41.1	0.14	−30	MIROC5	16.9 ± 1.0	38.7	0.07	−7
MPI-ESM-2-LR	19.5 ± 1.2	48.0	0.53	−14	MPI-ESM-LR	19.6 ± 1.2	39.0	0.12	0
MRI-ESM2-0	18.7 ± 1.4	43.6	0.51	−13	MRI-ESM1	14.4 ± 0.8	41.1	0.65	0
NorESM2-MM	22.2 ± 1.0	43.3	0.39	0	NorESM1-M	30.9 ± 0.8	46.7	0.37	−4
Mean	**(18.6 ± 4.2) ± (1.4 ± 0.5)**	**41.8**	**0.35**	**−12.7**	**Mean**	**(17.5 ± 4.7) ± (1.0 ± 0.3)**	**39.5**	**0.41**	**−8.3**

References

Caesar, L., Rahmstorf, S., Robinson, A., Feulner, G., Saba, V., 2018. Observed fingerprint of a weakening Atlantic Ocean overturning circulation. Nature 556 (7700), 191–196.

Capotondi, A., Alexander, M.A., Bond, N.A., Curchitser, E.N., Scott, J.D., 2012. Enhanced upper ocean stratification with climate change in the CMIP3 models. J. Geophys. Res.: Oceans 117 (C4).

Chen, X., Tung, K.K., 2018. Global surface warming enhanced by weak Atlantic overturning circulation. Nature 559 (7714), 387–391.

Cheng, J., Liu, Z., Zhang, S., Liu, W., Dong, L., Liu, P., Li, H., 2016. Reduced interdecadal variability of Atlantic meridional overturning circulation under global warming. Proc. Natl. Acad. Sci. USA 113 (12), 3175–3178.

Cheng, W., Chiang, J.C., Zhang, D., 2013. Atlantic meridional overturning circulation (AMOC) in CMIP5 models: RCP and historical simulations. J. Clim. 26 (18), 7187–7197.

Cunningham, S.A., Kanzow, T., Rayner, D., Baringer, M.O., Johns, W.E., Marotzke, J., Longworth, H.R., Grant, E.M., Hirschi, J.J.M., Beal, L.M., Meinen, C.S., 2007. Temporal variability of the Atlantic meridional overturning circulation at 26.5 N. Science 317 (5840), 935–938.

Davini, P., D'Andrea, F., 2016. Northern Hemisphere atmospheric blocking representation in global climate models: twenty years of improvements? J. Clim. 29 (24), 8823–8840.

Delworth, T.L., Zeng, F., 2016. The impact of the North Atlantic oscillation on climate through its influence on the Atlantic meridional overturning circulation. J. Clim. 29 (3), 941–962. https://doi.org/10.1175/jcli-d-15-0396.1.

Danabasoglu, G., Large, W.G., Briegleb, B.P., 2010. Climate impacts of parameterized Nordic Sea overflows. J. Geophys. Res.: Oceans 115 (C11). https://doi.org/10.1029/2010JC006243.

Drijfhout, S., 2015. Competition between global warming and an abrupt collapse of the AMOC in Earth's energy imbalance. Sci. Rep. 5 (1), 1–12.

Duchez, A., Hirschi, J.M., Cunningham, S.A., Blaker, A.T., Bryden, H.L., de Cuevas, B., Atkinson, C.P., McCarthy, G.D., Frajka-Williams, E., Rayner, D., Smeed, D., 2014. A new index for the Atlantic meridional overturning circulation at 26° N. J. Clim. 27 (17), 6439–6455.

Eyring, V., Bony, S., Meehl, G.A., Senior, C.A., Stevens, B., Stouffer, R.J., Taylor, K.E., 2016. Overview of the coupled model intercomparison project phase 6 (CMIP6) experimental design and organization. Geosci. Model Dev. (GMD) 9 (5), 1937–1958.

Frajka-Williams, Eleanor, et al., 2019. Atlantic Meridional Overturning Circulation: Observed Transport and Variability. Front. Mar. Sci. 6, 1–18.

Fraser, N.J., Cunningham, S.A., 2021. 120 years of AMOC variability reconstructed from observations using the Bernoulli inverse. Geophys. Res. Lett. 48 (18), e2021GL093893.

Gong, X., Knorr, G., Lohmann, G., Zhang, X., 2013. Dependence of abrupt Atlantic meridional ocean circulation changes on climate background states. Geophys. Res. Lett. 40 (14), 3698–3704.

Gong, X., Zhang, X., Lohmann, G., Wei, W., Zhang, X., Pfeiffer, M., 2015. Higher Laurentide and Greenland ice sheets strengthen the North Atlantic ocean circulation. Clim. Dynam. 45 (1), 139–150.

Haskins, R.K., Oliver, K.I., Jackson, L.C., Drijfhout, S.S., Wood, R.A., 2019. Explaining asymmetry between weakening and recovery of the AMOC in a coupled climate model. Clim. Dynam. 53 (1), 67–79.

Heuzé, C., 2017. North Atlantic deep water formation and AMOC in CMIP5 models. Ocean Sci. 13 (4), 609–622.

Hirschi, J.J.M., Barnier, B., Böning, C., Biastoch, A., Blaker, A.T., Coward, A., Danilov, S., Drijfhout, S., Getzlaff, K., Griffies, S.M., Hasumi, H., 2020. The Atlantic meridional overturning circulation in high-resolution models. J. Geophys. Res.: Oceans 125 (4), e2019JC015522.

Honjo, S., Eglinton, T.I., Taylor, C.D., Ulmer, K.M., Sievert, S.M., Bracher, A., German, C. R., Edgcomb, V., Francois, R., Iglesias-Rodriguez, M.D., Van Mooy, B., 2014. Understanding the role of the biological pump in the global carbon cycle: an imperative for ocean science. Oceanography 27 (3), 10–16.

Hu, A., Van Roekel, L., Weijer, W., Garuba, O.A., Cheng, W., Nadiga, B.T., 2020. Role of AMOC in transient climate response to greenhouse gas forcing in two coupled models. J. Clim. 33 (14), 5845–5859.

Huang, N.E., Wu, Z., 2008. A review on Hilbert-Huang transform: method and its applications to geophysical studies. Rev. Geophys. 46 (2).

Jha, B., Hu, Z.Z., Kumar, A., 2014. SST and ENSO variability and change simulated in historical experiments of CMIP5 models. Clim. Dynam. 42 (7–8), 2113–2124.

Johns, W.E., Baringer, M.O., Beal, L.M., Cunningham, S.A., Kanzow, T., Bryden, H.L., Hirschi, J.J.M., Marotzke, J., Meinen, C.S., Shaw, B., Curry, R., 2011. Continuous, array-based estimates of Atlantic Ocean heat transport at 26.5 N. J. Clim. 24 (10), 2429–2449.

Kageyama, M., Harrison, S.P., Kapsch, M.L., Löfverström, M., Lora, J.M., Mikolajewicz, U., Sherriff-Tadano, S., Vadsaria, T., Abe-Ouchi, A., Bouttes, N., Chandan, D., 2021. The PMIP4-CMIP6 Last Glacial Maximum experiments: preliminary results and comparison with the PMIP3-CMIP5 simulations. Clim. Past 17, 1065–1089.

Kanzow, T., Cunningham, S.A., Johns, W.E., Hirschi, J.J., Marotzke, J., Baringer, M.O., Meinen, C.S., Chidichimo, M.P., Atkinson, C., Beal, L.M., Bryden, H.L., 2010. Seasonal variability of the Atlantic meridional overturning circulation at 26.5 N. J. Clim. 23 (21), 5678–5698.

Keenlyside, N.S., Latif, M., 2007. Understanding equatorial Atlantic interannual variability. J. Clim. 20 (1), 131–142.

Kim, W.M., Yeager, S., Chang, P., Danabasoglu, G., 2018. Low-frequency North Atlantic climate variability in the community Earth system model large ensemble. J. Clim. 31 (2), 787–813.

Knutti, R., Sedláček, J., 2013. Robustness and uncertainties in the new CMIP5 climate model projections. Nat. Clim. Change 3 (4), 369–373.

Latif, M., Grötzner, A., 2000. The equatorial Atlantic oscillation and its response to ENSO. Clim. Dynam. 16 (2), 213–218.

McCarthy, G., et al., 2015. Ocean impact on decadal Atlantic climate variability revealed by sea-level observations. Nature 58, 508–510.

Menary, M.B., Roberts, C.D., Palmer, M.D., Halloran, P.R., Jackson, L., Wood, R.A., Mueller, W.A., Matei, D., Lee, S.K., 2013. Mechanisms of aerosol-forced AMOC variability in a state of the art climate model. J. Geophys. Res.: Oceans 118 (4), 2087–2096.

Nielsen, S.B., Jochum, M., Pedro, J.B., Eden, C., Nuterman, R., 2019. Two-timescale carbon cycle response to an AMOC collapse. Paleoceanogr. Paleoclimatol. 34 (4), 511–523.

Oka, A., Hasumi, H., Abe-Ouchi, A., 2012. The thermal threshold of the Atlantic meridional overturning circulation and its control by wind stress forcing during glacial climate. Geophys. Res. Lett. 39 (9).

O'Neill, B.C., Kriegler, E., Riahi, K., et al., 2014. A new scenario framework for climate change research: the concept of shared socioeconomic pathways. Climatic Change 122, 387–400.

Otto-Bliesner, B.L., Hewitt, C.D., Marchitto, T.M., Brady, E., Abe Ouchi, A., Crucifix, M., Murakami, S., Weber, S.L., 2007. Last Glacial Maximum ocean thermohaline circulation: PMIP2 model intercomparisons and data constraints. Geophys. Res. Lett. 34 (12).

Parker, A., Ollier, C.D., 2016. There is no real evidence for a diminishing trend of the Atlantic meridional overturning circulation. J. Ocean Eng. Sci. 1 (1), 30–35.

Peings, Y., Simpkins, G., Magnusdottir, G., 2016. Multidecadal fluctuations of the North Atlantic Ocean and feedback on the winter climate in CMIP5 control simulations. J. Geophys. Res. Atmos. 121 (6), 2571–2592.

Rahmstorf, S., Box, J.E., Feulner, G., Mann, M.E., Robinson, A., Rutherford, S., Schaffernicht, E.J., 2015. Exceptional twentieth-century slowdown in Atlantic Ocean overturning circulation. Nat. Clim. Change 5 (5), 475–480.

Roberts, C.D., Jackson, L., McNeall, D., 2014. Is the 2004–2012 reduction of the Atlantic meridional overturning circulation significant? Geophys. Res. Lett. 41 (9), 3204–3210.

Roberts, M.J., Jackson, L.C., Roberts, C.D., Meccia, V., Docquier, D., Koenigk, T., Wu, L., 2020. Sensitivity of the Atlantic meridional overturning circulation to model resolution in CMIP6 HighResMIP simulations and implications for future changes. J. Adv. Model. Earth Syst. 12 (8).

Rossby, T., Chafik, L., Houpert, L., 2020. What can hydrography tell us about the strength of the Nordic Seas MOC over the last 70 to 100 years? Geophys. Res. Lett. 47 (12), e2020GL087456.

Seip, K.L., Grøn, Ø., Wang, H., 2019. The North Atlantic oscillations: cycle times for the NAO, the AMO and the AMOC. Climate 7 (3), 43.

Sidorenko, D., Danilov, S., Streffing, J., Fofonova, V., Goessling, H.F., Scholz, P., Jung, T., 2021. AMOC variability and watermass transformations in the AWI climate model. J. Adv. Model. Earth Syst. 13 (10), e2021MS002582.

Smeed, D.A., et al., 2018. The North Atlantic Ocean Is in a State of Reduced Overturning. Geophys. Res. Lett. 45, 1527–1533.

Stouffer, R.J., Yin, J., Gregory, J.M., Dixon, K.W., Spelman, M.J., Hurlin, W., Weaver, A. J., Eby, M., Flato, G.M., Hasumi, H., Hu, A., 2006. Investigating the causes of the response of the thermohaline circulation to past and future climate changes. J. Clim. 19 (8), 1365–1387.

Talley, L.D., Reid, J.L., Robbins, P.E., 2003. Data-based meridional overturning streamfunctions for the global ocean. J. Clim. 16 (19), 3213–3226.

Tatebe, H., Ogura, T., Nitta, T., Komuro, Y., Ogochi, K., Takemura, T., Sudo, K., Sekiguchi, M., Abe, M., Saito, F., Chikira, M., 2019. Description and basic evaluation of simulated mean state, internal variability, and climate sensitivity in MIROC6. Geosci. Model Dev. (GMD) 12 (7), 2727–2765.

Taylor, K.E., Stouffer, R.J., Meehl, G.A., 2012. An overview of CMIP5 and the experiment design. Bull. Am. Meteorol. Soc. 93 (4), 485–498.

Thornalley, D.J., Oppo, D.W., Ortega, P., Robson, J.I., Brierley, C.M., Davis, R., Hall, I.R., Moffa-Sanchez, P., Rose, N.L., Spooner, P.T., Yashayaev, I., 2018. Anomalously weak Labrador Sea convection and Atlantic overturning during the past 150 years. Nature 556 (7700), 227–230.

Tung, K.K., Chen, X., 2018. Understanding the recent global surface warming slowdown: a review. Climate 6 (4), 82.

Van Vuuren, D.P., Riahi, K., 2011. The relationship between short-term emissions and long-term concentration targets. Clim. Change 104 (3), 793–801.

Vellinga, M., Wood, R.A., 2008. Impacts of thermohaline circulation shutdown in the twenty-first century. Climatic Change 91 (1), 43–63.

Wang, X., Li, J., Sun, C., Liu, T., 2017. NAO and its relationship with the Northern Hemisphere mean surface temperature in CMIP5 simulations. J. Geophys. Res. Atmos. 122 (8), 4202–4227.

Weijer, W., Cheng, W., Garuba, O.A., Hu, A., Nadiga, B.T., 2020. CMIP6 models predict significant 21st century decline of the Atlantic Meridional Overturning Circulation. Geophys. Res. Lett. 47 (12), e2019GL086075.

Wen, N., Frankignoul, C., Gastineau, G., 2016. Active AMOC–NAO coupling in the IPSL-CM5A-MR climate model. Clim. Dynam. 47 (7), 2105–2119.

Wu, Z., Huang, N.E., 2009. Ensemble empirical mode decomposition:A noise-assisted data analysis method. Adv. Adapt. Data Anal. 1 (1), 1–41.

Xu, X., Chassignet, E.P., Wang, F., 2019. On the variability of the Atlantic meridional overturning circulation transports in coupled CMIP5 simulations. Clim. Dynam. 52 (11), 6511–6531.

Yan, X., Zhang, R., Knutson, T.R., 2018. Underestimated AMOC variability and implications for AMV and predictability in CMIP models. Geophys. Res. Lett. 45 (9), 4319–4328.

Yeager, S., Danabasoglu, G., 2012. Sensitivity of Atlantic meridional overturning circulation variability to parameterized Nordic Sea overflows in CCSM4. J. Clim. 25 (6), 2077–2103.

Zebiak, S.E., 1993. Air–sea interaction in the equatorial Atlantic region. J. Clim. 6 (8), 1567–1586.

Zhang, X., Lohmann, G., Knorr, G., Xu, X., 2013. Different ocean states and transient characteristics in Last Glacial Maximum simulations and implications for deglaciation. Clim. Past 9 (5), 2319–2333.